Journal of the European Ceramic Society 19 (1999) 2529–2541

PII: S0955-2219(99)00124-7
0955-2219/99/$ - see front matter

High Temperature Single Crystal Properties of Mullite

W. M. Kriven, [a]* J. W. Palko, [a] S. Sinogeikin, [b] J. D. Bass, [b] A. Sayir, [c] G. Brunauer, [d] H. Boysen, [d] F. Frey [d] and J. Schneider [d]

[a]Department of Materials Science and Engineering, University of Illinois at Urbana-Champaign, Urbana, IL, USA
[b]Department of Geology, University of Illinois at Urbana-Champaign, Urbana, IL, USA
[c]NASA Glenn Research Center, Cleveland, OH, USA
[d]Institut für Kristallographie und Angewandte Mineralogie, Ludwig Maximilians Universität, München, Germany

Abstract

Extensive neutron diffraction and Rietveld studies of dense, hot pressed mullite ($3Al_2O_3{\cdot}2SiO_2$) have been conducted up to 1650 °C in air, yielding a complete set of lattice parameters and axial thermal expansion coefficients. Unconstrained powders of the same stoichiometric composition were also analyzed by X-ray diffraction and Rietveld techniques up to 900 °C in air, from which lattice parameters and thermal expansion coefficients were obtained. An earlier reported structural discontinuity was confirmed by XRD to lie in the temperature range 425 to 450 °C. Single-crystalline mullite fibers of composition $2{\cdot}5Al_2O_3{\cdot}SiO_2$ were grown from the melt by a laser-heated, float zone method. A partial set of the single-crystal elastic moduli were determined from various sections of fiber, by Brillouin spectroscopy, from room temperature up to 1400 °C. They indicated a roughly 10% reduction in stiffness over that temperature range. © *1999 Elsevier Science Ltd. All rights reserved.*

Keywords: elastic modulus, fibers, X-ray methods, thermal expansion, mullite.

1 Introduction

In the design of oxidation resistant, high temperature ceramic composites, it is wise to know the intrinsic properties of the component materials, independent of their structural configuration in the composite. Detailed theoretical predictions of composite behavior, particularly at elevated temperatures, would rely heavily on a knowledge of single crystal properties. Furthermore, since the fabrication and mechanical evaluation of composites is a difficult, time consuming and costly procedure, any data on the intrinsic properties of a component material is extremely valuable in accelerating the design, modelling and development of high temperature composites.

Mullite, of nominal composition ($3Al_2O_3{\cdot}2SiO_2$), is a highly attractive candidate for oxide composites.[1] As a matrix it is a widespread 'workhorse' refractory material, having very good creep resistance and chemical stability up to 1600 °C. The current, widely accepted phase diagram indicates that the equilibrium phase grown by solid state reaction has a narrow solid solution range around the $3Al_2O_3{\cdot}2SiO_2$ (abbreviated 3:2) composition.[2] However, when grown from the melt, mullite crystallizes in $2Al_2O_3{\cdot}SiO_2$ or 2:1 composition.[2] The solid solution range can further be extended to $3Al_2O_3{\cdot}SiO_2$ or 3:1 composition by rapid cooling in a closed container, in the absence of alumina nuclei.[2,3]

Currently, steady progress is being made in the production of mullite fibers. Directionally solidified mullite fibers can be grown by a laser heated, float-zone method.[4] They appear to consist of columns of single crystals with [c] axes parallel to the fiber direction. Polycrystalline mullite–alumina fibers (Nextel 720, from 3M Company, St. Paul, MN) have also been fabricated by a sol–gel process from an 85 wt Al_2O_3–15 wt. SiO_2 composition, which subsequently converts on firing at 1350 °C to 59 vol% mullite and 41 vol% Al_2O_3.[5] The microstructure is extremely fine grained with $\sim 0{\cdot}5\,\mu$m mullite grains containing < 100 nm largely intragranular alumina grains. This microstructure is unstable above 1300 °C however, due to grain growth and drastic loss of mechanical strength from an initial 2·4 MPa.[6,7] More recently, homogeneous, aluminosilicate, glass fibers (of mullite composition) and amorphous yttrium aluminate fibers (of $Y_3Al_5O_{12}$ or 'YAG' composition) have been pulled from deeply undercooled melts via a

*To whom correspondence should be addressed. Fax: +1-217-333-2736.

containerless processing technique.[8,9] The high tensile strengths of the aluminosilicate glass fibers (~6 GPa) however, are again drastically reduced to 1 GPa at best, due to uncontrolled random crystallization to mullite or YAG, on annealing above 1100 °C. Work is therefore in progress to develop textured or single crystal fibers from the amorphous solid precursors.

1.1 Crystallographic measurements

Measurements of the thermal expansion of various mullite compositions are mainly reported for temperatures up to 900 °C and are either based on dilatometric measurements or on X-ray diffraction.[10–14] For higher temperatures reliable data are rare.[13] It has to be kept in mind that the former, i.e. the dilatometric method provides results which are always of both structural and microstructural origin and therefore, an average, which is hard to interpret on an atomic length scale. X-ray diffraction allows, at least in principle, a separation of both aspects via an evaluation of the positions of the reflections in a diffraction pattern and by a line profile analysis. The X-ray method has its limits if the sample material is coarse grained, which is sometimes unavoidable, and because of absorption effects. In particular in the high temperature regime around and above 1000 °C, the X-ray diffraction method becomes additionally tedious for experimental reasons.

An alternative diffraction method uses neutrons. In the case of mullite neutron diffraction, results are not affected by absorption and the relatively large sample volume allows for good statistics, even in the case of coarse grained samples. Moreover, the oxygens have a relatively high scattering power for neutrons so that oxygen related structural details can be studied in oxide compounds more reliably. We performed in-situ neutron diffraction experiments with the 3:2 mullite described above up to a temperature of 1650 °C. The overall aim of the investigation was a full structure refinement of mullite at high temperatures. Only the thermal expansion results of neutron diffraction measurements will be given here, since full information will be published in a forthcoming paper.[15]

1.2 Elastic constant measurements

1.2.1 Bulk properties

The bulk elastic properties of mullite have been measured on sintered compacts of relatively pure, raw materials.[16,17] More recent work on hot pressed stoichiometric 3:2 mullite, which was hydrothermally grown without any glassy phase, indicated an unusual decrease in Poisson's ratio with increasing temperature up to room temperature.[18] This was attributed to the incommensurate modulation in the mullite crystal structure. Early high temperature measurements[16] of relatively pure raw materials indicate a drop in elastic modulus for both 3:2 and 2:1 mullite above 600 °C, strongly suggesting the presence of intergranular glass. With the availability of highly textured, polycrystalline fibers,[4] it was decided to measure the elastic moduli of mullite up to temperatures of 1400 °C.

1.2.2 Single crystal properties

The complete elasticity tensor can be measured by the Brillouin light scattering technique.[19] This technique presents several advantages over other methods, the most important being that only very small samples are required, no contact is needed with the sample, and it is suitable for low-symmetry crystals. The sample size is limited only by the spot size of the laser used as the excitation source, making Brillouin scattering well-suited for measurements on the thin mullite fibers used in this study. Also, only optical access to the sample is required for Brillouin measurements, which allows much flexibility in furnace design.

Brillouin scattering involves the inelastic scattering of light from phonons in a crystal. If V is the velocity of the phonon, ϕ and ϕ' are the incident and scattered angles, respectively, and ν and ν' are the frequencies of the incident and scattered photons, respectively, then the equation relating phonon velocity to the frequency shift of the scattered photon, $\Delta\nu = \nu' - \nu$, is

$$V = \left(\frac{\Delta\nu}{\nu}\right)\left(\frac{c}{2n\sin\phi}\right) \tag{1}$$

for the case of symmetric scattering where ϕ and ϕ' are very nearly equal. c is the speed of light in vacuum and n is the refractive index for the direction of photon propagation. In this experiment we use a 'platelet geometry',[20] which allows $n\sin\phi$ to be replaced by $n_o\sin\theta_o$, where n_o is the index of the surrounding medium, and θ_o the incidence angle of the laser light. Platelet geometry allows access to all phonon directions in the plane of the sample.

The velocities of acoustic phonons are determined entirely by the elastic moduli and density of the material. The velocity in eqn (1) for plane monochromatic waves must satisfy Christoffel's equation [eqn (2)].[21]

$$\left|C_{iklm}q_iq_m - \rho V^2\delta_{kl}\right| = 0 \tag{2}$$

where q_i and q_m are unit vectors in the phonon propagation direction, ρ is the density, and C_{ijkl} is the elastic tensor.

1.3 Objective

In anticipation of the successful growth of single crystal or aligned textured fibers of mullite, the work described here was undertaken. The goal of a mullite matrix reinforced with mullite fibers coated by a suitable debonding oxide interphase would be well served by a precise knowledge of crystallographic lattice parameters as a function of temperature up to 1600 °C, as well as axial and volumetric thermal expansion coefficients. These data would enable the residual stresses arising during high temperature cycling to be estimated. Since dense mullite composites could be used as shingles to line an aircraft combustion chamber, for example, (Ref. 22 and H. Schneider, German Aerospace Center, pers. comm.) the thermal expansion of dense, hot pressed, polycrystalline mullite samples were measured, rather than of loose powders, as is customary in crystallographic measurements by X-ray or neutron diffraction. In addition, 3:2 mullite powder would be studied by X-ray diffraction up to 900 °C, and the data would be analyzed by Rietveld methods.

To complement the crystallographic data, and enable better modelling of the high temperature behavior of a mullite-containing composite, single crystal elastic moduli for orthorhombic mullite would be determined experimentally. Brillouin spectroscopic measurements would be made both at room temperature, and up to 1400 °C. Information gathered from this work would then indicate the feasibility and limits of using mullite fiber-reinforced composites in a load-bearing structural application, at high temperature in an oxidizing environment.

2 Experimental Procedures

2.1 Sample fabrication

For diffraction studies, hydrothermally grown, stoichiometric 3:2 mullite powder (Kyoritsu Ceramic Materials Co. Ltd., Tsukisan-cho 2-41, Minato-ku, Nagoya 455-91, Japan) was used as a starting material. For X-ray diffractometry, the powder of average particle size 0·3 μm was inserted into 0·3 mm diameter quartz capillaries which were kept in rotation during the measurements at all temperatures to reduce preferred orientation effects. For neutron diffraction, a polycrystalline mullite ceramic specimen was prepared by hot pressing to full density under vacuum, at 1600 °C and 34 MPa for 1 h, in a 3 inch bore graphite die with graphite spacers and plungers.[18,23]

For elastic constant measurements, mullite fibers of $\sim$500 μm diameter were grown from starting compositions close to the 3:2 composition from high purity CERAC® pure (99·99% pure, 325 mesh) polycrystalline alumina powder (Ceralox Corp., Tucson, AZ 08576) and 99·99% pure SiO_2 from Alpha Products. The extruded mixture was made into a feeder rod in a laser heated, floating zone apparatus which was a fully automated, computer-controlled fiber processing facility at the NASA Glenn Research Center. The fiber pulling technique is fully described elsewhere.[4]

2.2 X-ray diffractometry

The X-ray powder diffraction experiments were performed on a focussing STOE-STADIP diffractometer equipped with a curved Ge(111) monochromator to produce strictly monochromatic Mo$K\alpha_1$ radiation. Data were collected using an overlapping stepscan mode of a linear position sensitive detector of about 5° acceptance angle and 0·02° channel width yielding 1500 data points in the 2θ-range from 5·5 to 35·5°. Each scan was repeated four times to monitor the stability of the intensity and the scans were then added together for better averaging. The resulting minimum half-width was 0·09° in 2θ. For measurements at elevated temperatures the computer controlled STOE furnace 0·65·1 was employed. The heating element consists of a current heated graphite tube holding the sample capillary vertically to the scattering plane. Bores in the graphite tube permitted unobstructed pathways for both the primary beam as well as for the scattered radiation. The temperature measured by a thermocouple in the graphite tube was kept constant to within 0·2°.

2.3 Neutron diffraction

The experiments were carried out at the powder diffractometer MANI at the FRM reactor facility in Munich and at the instrument D2B of the HFR/ILL in Grenoble. The diffraction patterns were recorded with a wavelength of 0·1594 nm. A mirror furnace was used which operated at ambient conditions in air. The neutron mirror furnace is based on light focussed by two rotational ellipsoids.[24] Two different experiments were carried out. The first one started with a $0{\cdot}8\times1\times1\,cm^3$ sample cut from freshly hot pressed material which had a dark color. Due to a malfunction of the temperature control system at about 1100 °C, the heating procedure was interrupted. After the break, the heating sequence was continued up to 1650 °C. As a by-product we observed a colour change of the sample from dark to white. In the second experiment the 'same' (white, i.e. non-pristine) sample was used. Here an uninterrupted heating (room temperature to 1650 °C) and cooling cycle down to 650 °C was employed.

2.4 Elastic constants measurements

Three platelet-shaped samples were cut from a single mullite fiber produced by the laser-heated float zone method.[4] The platelets were ground nominally parallel to (010), (100), and (001) planes. The former two were oriented lengthwise with respect to the fiber, whereas the later was a cross section.

An Ar^+ laser at a power of < 200 mW was used for ambient temperature measurements. At high temperature, up to 400 mW were used to maximize the Brillouin signal, since sample heating was not a concern. Light scattered at 90° from the incident beam, was analyzed by a 6 pass, tandem Fabry–Perot interferometer and photomultiplier tube (PMT).[25] Figure 1 shows a representative spectrum in which Stokes and anti-Stokes Brillouin peaks occur symmetrically about the strong Rayleigh peak. The peaks labeled 'ghost' are the adjacent orders of Rayleigh scattered light which are reduced in amplitude by $> 10^3$ by the tandem interferometer. The distance from the Rayleigh peak to the Brillouin peaks is taken to be the frequency shift for that mode.

A set of elastic constants were obtained by a least-squares procedure which minimized misfit between measured velocities and those calculated from the elastic constants.[26] For the high temperature measurements, elastic moduli were calculated directly from Christoffel's equation[21] using the average velocity for each temperature and direction.

3 Results

3.1 X-ray diffraction

Rietveld refinement was performed for all data sets to extract the temperature dependence of the cell dimensions. The refinement was performed in space group *Pbam*, and published room temperature atom coordinates[27] were used as starting values. The resulting cell dimensions and the corresponding cell volumes are given in Table 1 and are shown Fig. 2(a)–(d). About 2 wt% of Al_2O_3 was detected as a minority phase, which could be neglected for the purpose of a cell parameter Rietveld refinement.

The cell dimensions of our X-ray data compared very well with previous data[14] obtained by the Guinier technique. Our cell parameters *b* and *c* deviated only by about 1 to 2 estimated standard deviations (e.s.d.s), whereas *a* deviated by about 6 e.s.d.s. The discontinuities of cell parameters *a* and *b* between 400°C and 500°C seen by Schneider *et al.*[14] were also found with this sample. The temperature range for the discontinuity could be narrowed down to between 425 and 450 °C. The discontinuity of *a* was found to be more pronounced than that of *b*, which was again in good agreement with previous literature.[14] All cell dimensions showed a marked lower thermal expansion between room temperature and 100 °C. Neglecting the (small) discontinuities around 435 °C, a linear thermal expansion may be fitted to the data from 100 up to 700 °C (presented in Table 2).

Above 700 °C, both *a* and *b* displayed a marked increase in thermal expansion and *c* showed a discontinuity. Cooling down from 900 °C to room temperature, both *a* and *b* adopted higher cell dimensions whereas *c* had a lower cell dimension, as compared to the values before the high temperature cycle.

3.2 Neutron diffraction

The measured data were analysed by the Rietveld technique using an extended version[28] of the program of Thomas and Bendall.[29] This meant that complete structure refinements were carried out for

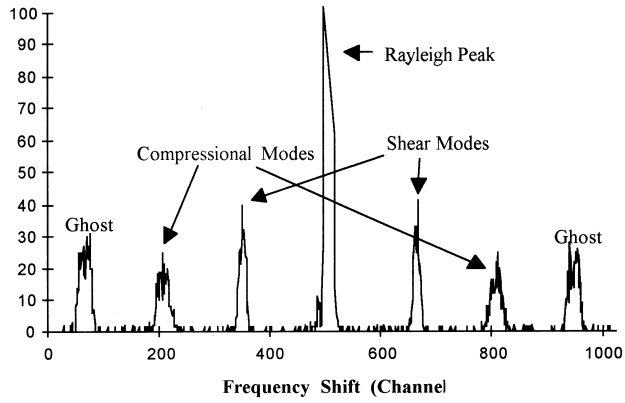

Fig. 1. A typical Brillouin spectrum, depicting the main Rayleigh peak symmetrically surrounded by Stokes and anti-Stokes peaks. The 'ghost' peaks are adjacent orders of Rayleigh scattered light which have been reduced by $> 10^3$ by the tandem Fabry–Perot interferometer.

Table 1. Cell dimensions of 3:2 Kyoritsu mullite powder as determined by X-ray diffraction and Rietvald analysis

Temperature (°C)	*a(Å)*	*b(Å)*	*c(Å)*	*Volume (Å³)*
29	7·5501(8)	7·6894(8)	2·8837	167·41
100	7·75506	7·6913	2·8845	167.51
200	7·5530	7·6958(9)	2·8858	167·74
300	7·5559	7·6995	2·8872	167·97
400	7·5579	7·7045	2·886	168·20
425	7·75588	7·7056	2·8889	168·27
450	7·5600(9)	7·7061	2·8893(3)	168·33(4)
475	7·5605	7·7073	2·8895	168·38
500	7·5613	7·7087	2·8898	168·44
600	7·5649(10)	7·7126(10)	2·8912	168·68
700	7·5668	7·7167	2·8927	168·91
800	7·5703	7·7221	2·8945	169·21
900	7·5742	7·7295(11)	2·8958	169·53
29	7·5508	7·6914	2·8830	167·43

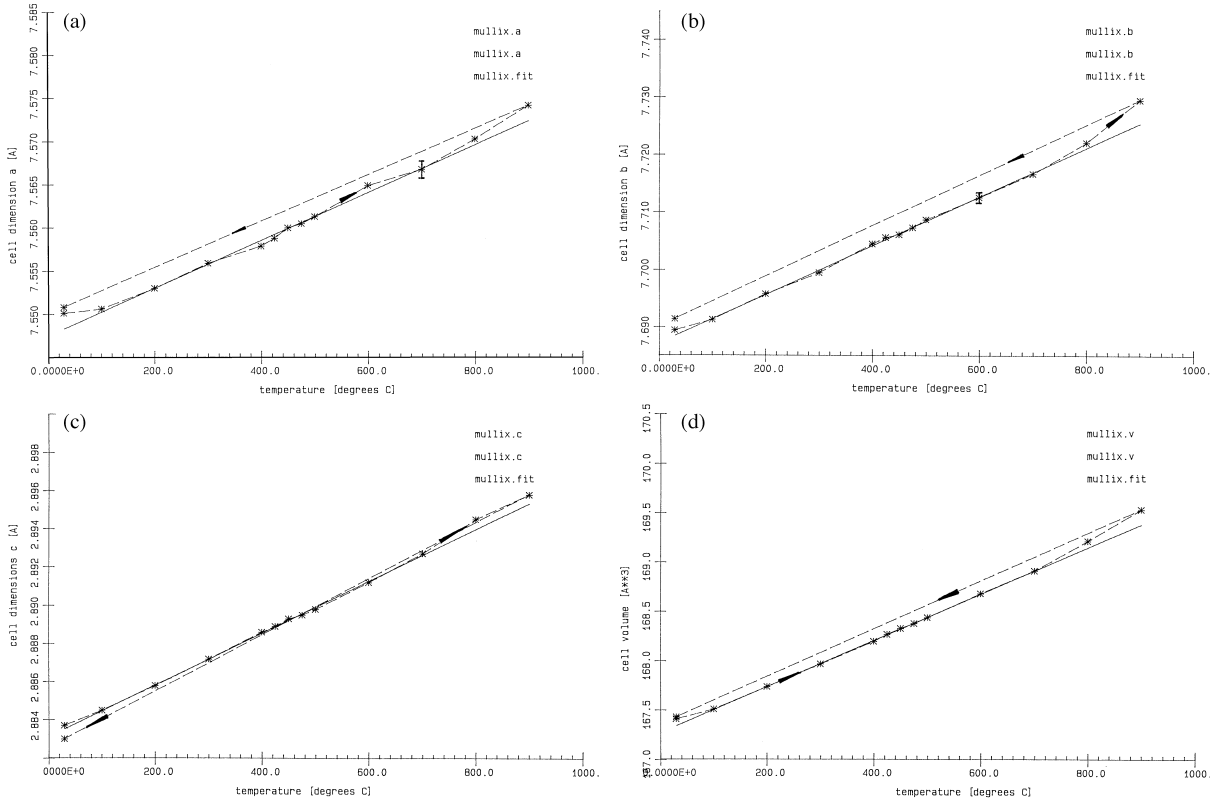

Fig. 2. Cell dimensions measured up to 900 °C by X-ray diffraction and Rietveld analysis, of stoichiometric $3Al_2O_3{\cdot}2SiO_2$ mullite powder. (a) *a*, (b) *b*, (c) *c*, (d) unit cell volume.

Table 2. Linear thermal expansion coefficients and volume expansion of 3:2 Kyoritsu mullite powder as determined by X-ray diffraction and Rietvald analysis

Cell dimensions (Å)	*Linear thermal expansion α (10⁻⁶/K) (100–700°C)*
a	3·7(2)
b	5·5(2)
c	4·7(2)
Volume = 1·4(1)×10⁻⁵ Å³	

each temperature point. The refinements were carried out within the orthorhombic space group *Pbam*. It is beyond the scope of this paper to discuss the structural changes in any detail. These are the subject of the forthcoming paper.[15] The lattice constants comprised three out of 48 refinable parameters which showed, as usual, only small correlations with the set of remaining structural parameters, such as atomic positions, fractional site occupations and atomic displacement parameters, as well as instrumental parameters related to the shape of the reflections.

Results for the lattice constants are given in Tables 3 and 4, and are shown in Fig. 3(a)–(d) as a function of temperature. The lines are only a guide to the eyes and refer to the different parts of the experiment as explained in the experimental procedures (Section 2.3). The agreement factors (precisely, the weighted profile R-factors R_{wp}) between observed and fitted data were around 12%, while the goodness-of-fit values ranged between 1·2 and 1·8. Fig. 3(d) shows the behaviour of the cell volume which is simply given by the product of a, b, and c in the orthorhombic crystal system. From these lattice parameters, the thermal expansion coefficients may be evaluated. In our case of the point group *mmm*, we had only three independent coefficients $\alpha_{ii}(i = 1, 2, 3)$ which may be evaluated from a, b, c by $\alpha_{11} = \frac{\Delta\alpha}{(\alpha\Delta T)}$, $\alpha_{22} = \frac{\Delta\beta}{(\beta\Delta T)}$, $\alpha_{33} = \frac{\Delta c}{(c\Delta T)}$, where T denotes the temperature. These values are included in Table 3. An average lattice expansion coefficient is defined by $\alpha = \frac{(\alpha_{11}+\alpha_{22}+\alpha_{33})}{3}$ and may be compared with values determined by macroscopic methods. One should keep in mind that here a is a structure-related coefficient and not affected by microstructural effects which are governed by the grain-microstructure in the sample. However, structural disorder, for example, produced by vacancies, do affect the α_{ii} or α. These remarks need to be considered when comparing published data for the thermal expansion of mullite.

3.3 Elastic constants determination

Optical microscopy of the laser heated, float zone mullite fibers[4] indicated a 'bamboo-like' columnar structure with a slightly elliptical cross section,

Table 3. (a) Lattice parameters a, b, c, thermal expansion coefficients α_{ii}, and the average thermal expansion $\alpha = (\alpha_{11} + \alpha_{22} + \alpha_{33})/3$ for hot pressed, as-received (grey) 3:2 mullite, as determined by neutron diffraction

Temperature (°K)	*a (Å)*	α_{11} *(10^{-6} K^{-1})*	*b (Å)*	α_{22} *(10^{-6} K^{-1})*	*c (Å)*	α_{33} *(10^{-6} K^{-1})*	α *(10^{-6} K^{-1})*
298	7·54350(9)	4·05	7·69404(8)	5·65	2·8841(4)	5·70	5·13
723	7·55654(9)	8·14	7·71365(8)	12·41	2·89116(4)	9·81	10·12
923	7·56887(11)	2·09	7·73285(11)	1·00	2·89685(4)	3·09	2·06
1023	7·57045(8)	6·86	7·73362(8)	9·73	2·89774(3)	8·34	8·31
1123	7·57565(9)	6·12	7·74115(9)	8·55	2·90019(4)	7·87	7·51
1173	7·57796(11)	6·25	7·74446(11)	8·49	2·90133(4)	9·00	7·91
1223	7·58033(11)	6·89	7·74775(11)	9·48	2·90264(4)	9·26	8·54
1273	7·58295(10)	6·34	7·75156(9)	10·16	2·90398(4)	7·41	7·97
1373	7·58776(12)		7·75944(11)		2·90613(5)		
(b) Corresponding data after cooling to room temperature and continued heating of air-annealed, (white) 3:2 mullite specimen							
923	7·56337(29)	4·45	7·71767(25)	6·14	2·89381(10)	5·63	5·80
1373	7·57854(25)	4·47	7·73904(23)	6·48	2·90115(9)	5·86	5·60
1473	7·58193(27)	4·59	7·74406(24)	6·47	2·90285(9)	5·40	5·49
1573	7·58541(29)	4·44	7·74907(26)	6·34	2·90442(10)	4·92	5·29
1673	7·58878(23)	5·83	7·75399(20)	9·50	2·90585(8)	6·50	7·28
1773	7·59320(15)	4·83	7·76137(13)	7·45	2·90774(5)	5·49	5·92
1823	7·59504(34)	12·33	7·76426(30)	13·13	2·90854(11)	10·14	11·87
1873	7·59973(22)	3·60	7·76936(20)	10·54	2·91002(7)	3·95	6·03
1923	7·60109(42)		7·77346(38)		2·91059(14)		

Table 4. Neutron diffraction data after second heating of hot pressed, air-annealed (white) 3:2 Kyoritsu mullite specimen

Temperature (°K)	*a (Å)*	*b (Å)*	*c (Å)*
298	7·54736(13)	7·69337(12)	2·88481(5)
723	7·55767(14)	7·70975(12)	2·89021(5)
923	7·56341(14)	7·71862(13)	2·893127(5)
1273	7·57392(15)	7·73401(14)	2·89833(5)
1573	7·58386(12)	7·74743(11)	2·90361(4)
1723	7·58963(18)	7·75566(16)	2·90619(6)
1773	7·59028(19)	7·75657(17)	2·90656(6)
1823	7·59353(20)	7·76253(18)	2·90804(7)
1873	7·59682(23)	7·76810(20)	2·90937(8)
1923	7·60026(25)	7·77305(22)	2·91057(8)
1823	7·59239(21)	7·76147(19)	2·90764(7)
1773	7·58933(20)	7·75694(17)	2·90645(7)
1573	7·58085(17)	7·74428(15)	2·90238(6)
923	7·56138(14)	7·71624(12)	2·89307(5)

reminiscent of an egg shape, with a facet at the bottom of the vertical 'egg'. The fiber was for the most part optically clear, with occasional white streaks across its width, consisting of bubbles or occlusions. These white streaks often coincided with joins of the 'bamboo segments'. The fiber showed uniform extinction along its length under cross polarized light, regardless of rotation about this axis. Extinction was less uniform in cross section, indicating that the fiber was somewhat polycrystalline. Separate X-ray diffraction measurements taken on a four circle diffractometer verified that the fiber consisted of multiple crystallites oriented in very nearly the same direction along the fiber axis. The X-ray data showed that the c axis was virtually coincident with the fiber axis for all the constituent crystallites. However the crystallites had slightly varying rotations about the c axis. All the crystallites lay within 5° of each other, where of those, the majority lay within 2° of each other. Lattice parameters for the sample were calculated by fitting the major peak for each reflection (Table 5). The calculated unit cell angles deviated slightly from 90° due to the small peaks close by, but this deviation was ignored in the calculation of cell volume.

Compositional analysis was made by wavelength dispersive spectroscopy (WDS) in an electron microprobe, and it indicated a mullite composition of $2{\cdot}5Al_2O_3{\cdot}SiO_2$, with a standard deviation of $\pm 0{\cdot}10$ in the molar ratio.

Using the formula $Al_{4+2x}Si_{2-2x}O_{10-x}$ from literature[30] for unit cell composition yielded an average theoretical density of $3{\cdot}10\,g\,cm^3$ at room temperature, which lay between the 2:1 and 3:1 compositional extremes. The densities for high temperature were determined from thermal expansions calculated with a quadratic curve fit to the relative cell volume as measured by neutron diffraction presented in Section 3.2 above, using only the aged sample data.

Figures 4(a)–(c) show the ambient temperature velocities measured for the (010), (100), and (001) platelets, respectively, and velocities calculated from the fitted elastic moduli. Rotation of the sample with respect to its crystal axes was determined by optical extinction under cross-polarized light. The elastic moduli obtained are listed in Table 6. They are considered to be accurate to

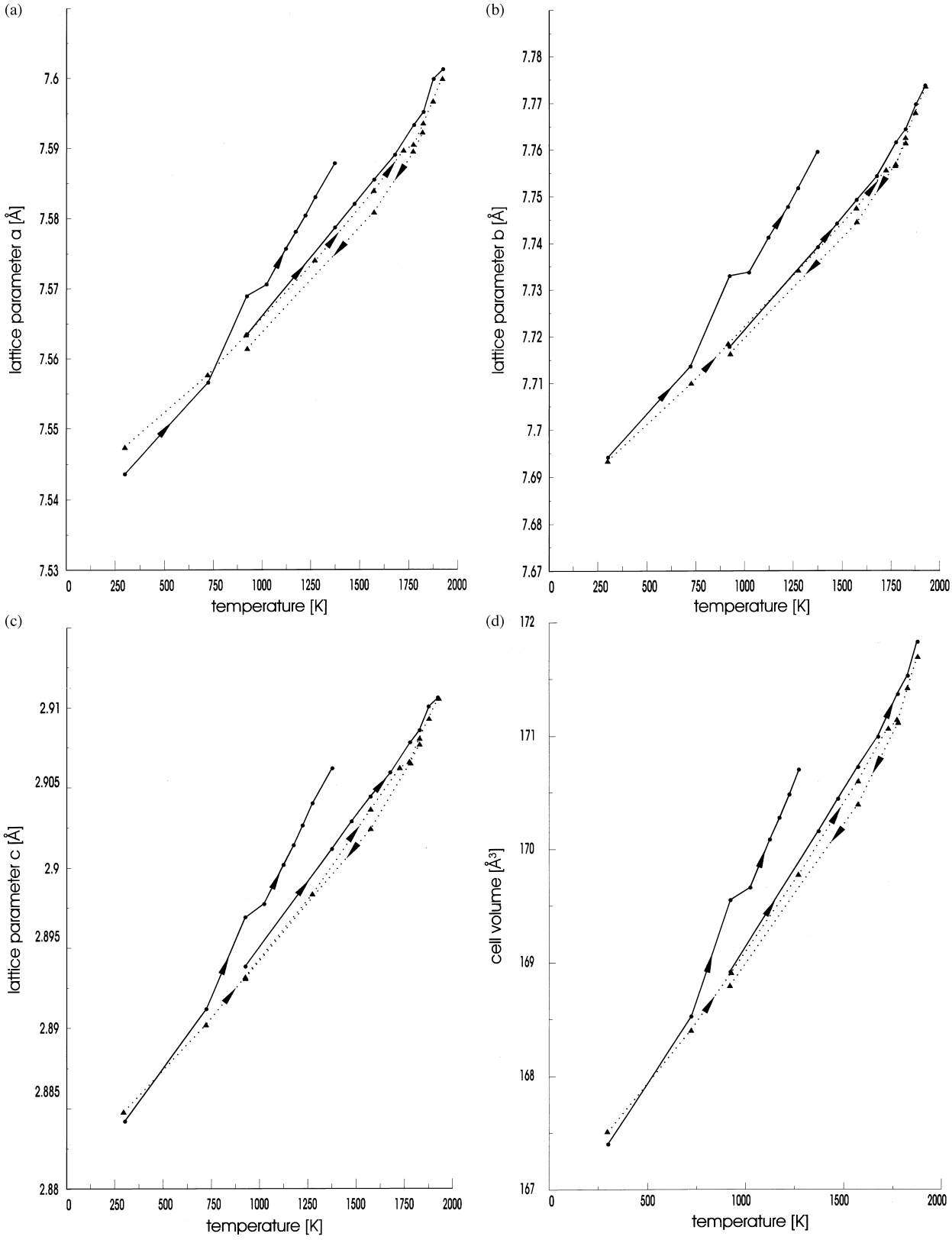

Fig. 3. Lattice parameters *a,b,c* and cell volume ($=a\times b\times c$) of mullite [(a) to (d), respectively], as a function of temperature. Full circles relate to the first experiment on grey mullite, triangles to the second experiment on annealed white mullite. Error bars are smaller than the symbols. The uncertainty of temperature was about ± 10 K. Solid and dotted lines are only guides to the eyes.

within $\pm 3\%$ which accounts for uncertainty in the calculated density, as well as possible misorientation of the crystals.

Velocity measurements were made along two directions in both the *a–c* and *b–c* crystallographic planes up to 1400 °C, in increments of 200 °C [Fig. 5(a) and (b)]. In these preliminary experiments, nominal temperatures are cited as read directly from the furnace temperature controller. However, even an error of 20°C yields an ~0·2% error in the

Table 5. Lattice parameters measured by X-ray diffractometry for mullite fiber grown by the laser-heated, float-zone method

a (Å)	7·58(1)
b (Å)	7·68(1)
c (Å)	2·90(1)
Cell volume (Å^3)	169(1)
Theoretical density (g cm^{-3})	3·10

Cij's. The moduli C_{11}, C_{33}, C_{44}, and C_{55} were calculated for each temperature [Figs. 6(a) and (b)].

The orientation of the sample at high temperature in a given crystallographic plane was determined from the longitudinal to shear velocity ratio $\left(\frac{V_l}{V_s}\right)$. Uncertainties in sample orientation and the thermal expansion increased the error of the high temperature elastic constants. At this point it is difficult to assign a formal uncertainty to the high temperature measurements due to the sparse preliminary data set, but current measurements in progress will allow a more rigorous assessment in the high temperature moduli.[31]

4 Discussions

4.1 X-ray diffraction

The fact that our data also showed the discontinuities of the lattice parameters a and b around 425 °C supports the general validity of this effect in mullite. Explanations were given in terms of the complex dependencies between thermal expansion and structural arrangement of mullite and the related phases andalusite and sillimanite. A relation to domains originating from oxygen vacancies was also discussed by Schneider *et al.*[14] The somewhat larger deviation of our cell parameter a may be related to the fact that this cell direction seems to be more sensitive to sample dependent variations, possibly oxygen vacancies and their related macrostrains. These effects may also be responsible for the heating cycle induced widening and flattening of the unit cell observed with our sample but not with the sample of Schneider *et al.*[14] A full multiphase Rietveld refinement including minority phases will be performed in the future in order to extract more accurate intensities to resolve structural details at the discontinuities mentioned above.

4.2 Neutron diffraction

Figure 3 reveals a striking result in that the behavior of the lattice constants of the pristine (grey) sample material differed appreciably from that of the pre-heated sample. This difference became remarkable at temperatures of about 700 °C. Above this temperature the material exhibited a different, i.e. stronger expansion as compared to the pre-heated sample (see below). This behavior was reflected by all three lattice constants. Note that after the first heating of the sample the colour changed to white. If the hypothesis is correct that the dark colour (of the pristine material) were due to a considerable amount of oxygen vacancies, this different expansion behavior would relate to a strongly disordered mullite structure. After annihilation of these vacancies we should then have a 'normal' expansion. This is evidenced by the coincidence of the values measured in two subsequent experiments and further supported by the full structural analysis.[15] Generally the thermal expansion was most pronounced in the b-direction and the lowest values occurred along the a-axis. The mean expansion coefficient (of the non-pristine, grey sample) was around $5{\cdot}5\times10^{-6}$ (K^{-1}) for temperatures up to 1550 °C. Except for the generally different expansion of the fresh (grey) sample, we observed an additional anomaly at around 700 °C. We refrain from further discussion because this observation is based only on one single temperature measurement, and must be supported by further detailed measurements. We do mention it, however, because some 'anomalies' are reported earlier for temperatures matching this temperature regime.[14] A second 'anomaly' might be in the high temperature regime between 1550 and 1600 °C (cf. Fig. 3 and Tables 3 and 4). Once again, this effect must be substantiated by further experiments. Comparing the two different runs with the heated sample there were only small differences, and, if any, a small hysteris on completing a full heating cooling cycle (cf. Fig. 3). We are not completely sure whether these small differences or 'hysteresis' are substantial or not, because we cannot fully exclude aging effects of the sample undergoing one or more heating cycles in air.

4.3 Elastic constants

Because of fiber microstructure, the elastic moduli probably represent an average over numerous crystallites. Since the crystallites have different rotations about their c axes, this effect is most important in the (001) plane. This plane shows relatively low anisotropy in phonon velocity, which is most likely real, since velocities are averaged over a range of orientations less than 5°. The low anisotropy in the (001) plane can be correlated to the crystal structure. Mullite may be considered as cross-linked, (edge-shared) chains of Al^{3+} octahedra and tetrahedral (corner-shared) chains containing alternating Si^{4+} and Al^{3+} cations, running parallel to the c axis.[32] Longitudinal and transverse vibrations polarized in this plane represent deformations of the voids and cross-linking bonds

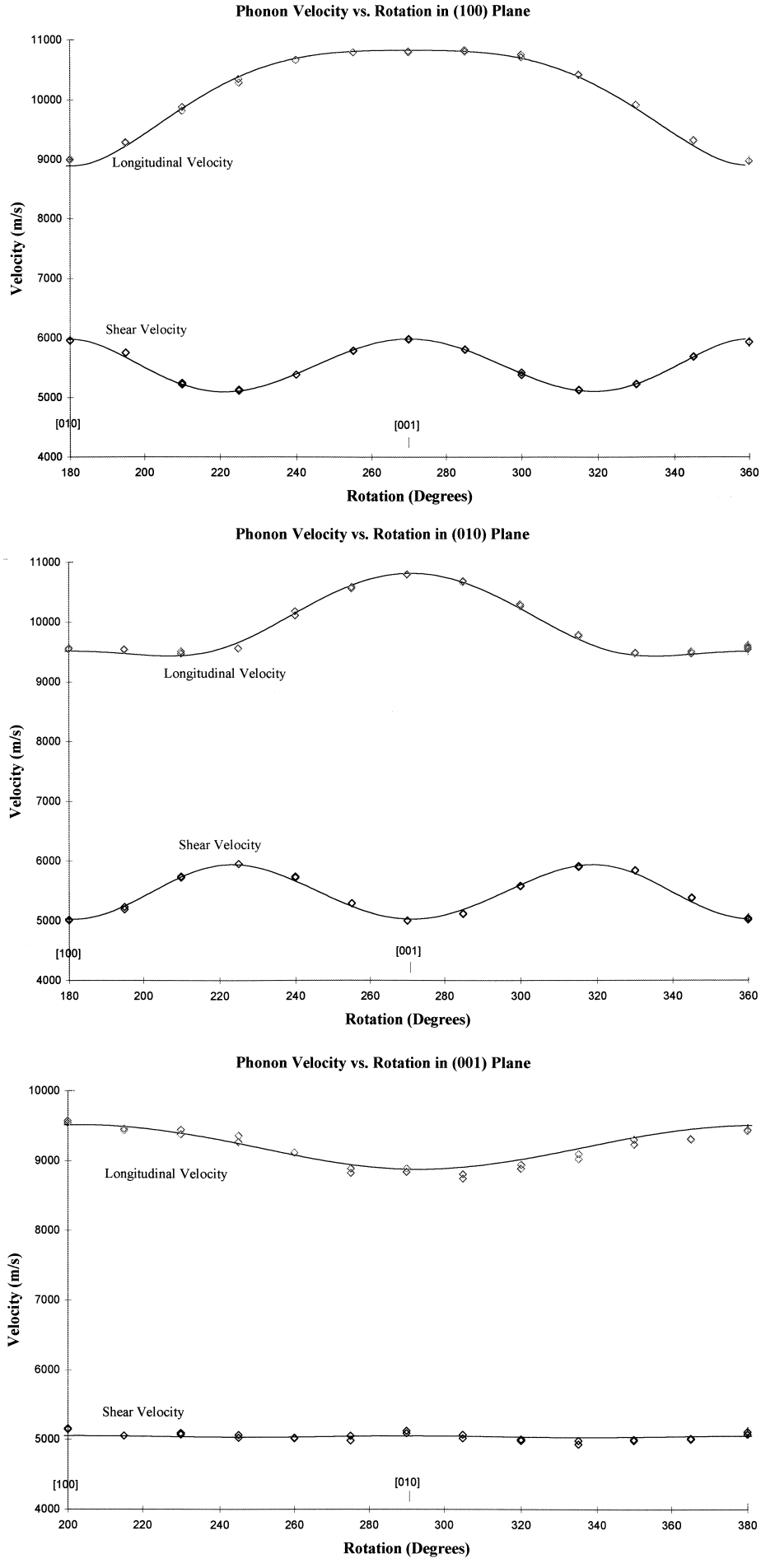

Fig. 4. Measured and fitted phonon velocities of mullite fiber in the (a) (100), (b) (010), and (c) (001) planes.

Table 6. Single crystal, room temperature, elastic moduli of mullite fiber grown by the laser heated, float-zone method

C_{11} (GPa)	280
C_{22} (GPa)	245
C_{33} (GPa)	362
C_{44} (GPa)	111
C_{55} (GPa)	78·1
C_{66} (GPa)	79·0
C_{12} (GPa)	105
C_{13} (GPa)	99·2
C_{23} (GPa)	135

between these chains regardless of directions. In the (100) and (010) planes, the nature of the deformations change from being normal to the polyhedral chains to being parallel to them, as the propagation direction approaches [001] for a longitudinal wave and vice versa for a shear wave polarized in the plane of rotation. This accounts for the higher anisotropy in these planes, since the polyhedral chains are relatively stiff along their length. This is evident from the substantially higher value of C_{33} as compared to C_{11} and C_{22}. Similar correlations have been shown for sillimanite and andalusite[33] which share structural similarities with mullite. The mullite sample measured did not contain a substantial amount of glassy phase as was thought to exist in the impure sample measured in previous work.[16,17] This accounts for the lack of marked decrease in moduli above 600 °C. Further work is in progress to completely specify the elastic tensor of mullite to 1400 °C.[31]

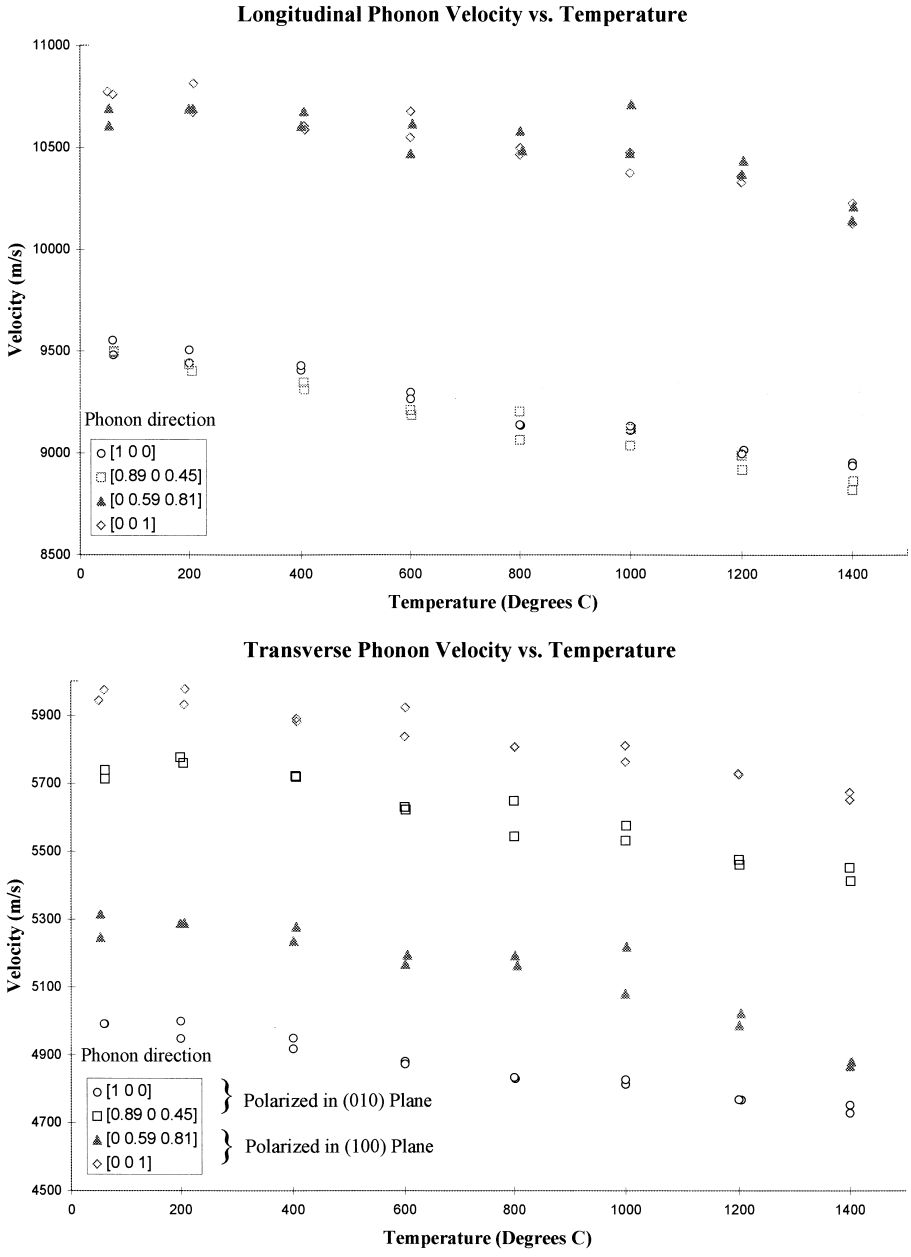

Fig. 5. Measured phonon velocities versus temperature for selected crystallographic directions. (a) longitudinal waves; (b) transverse waves.

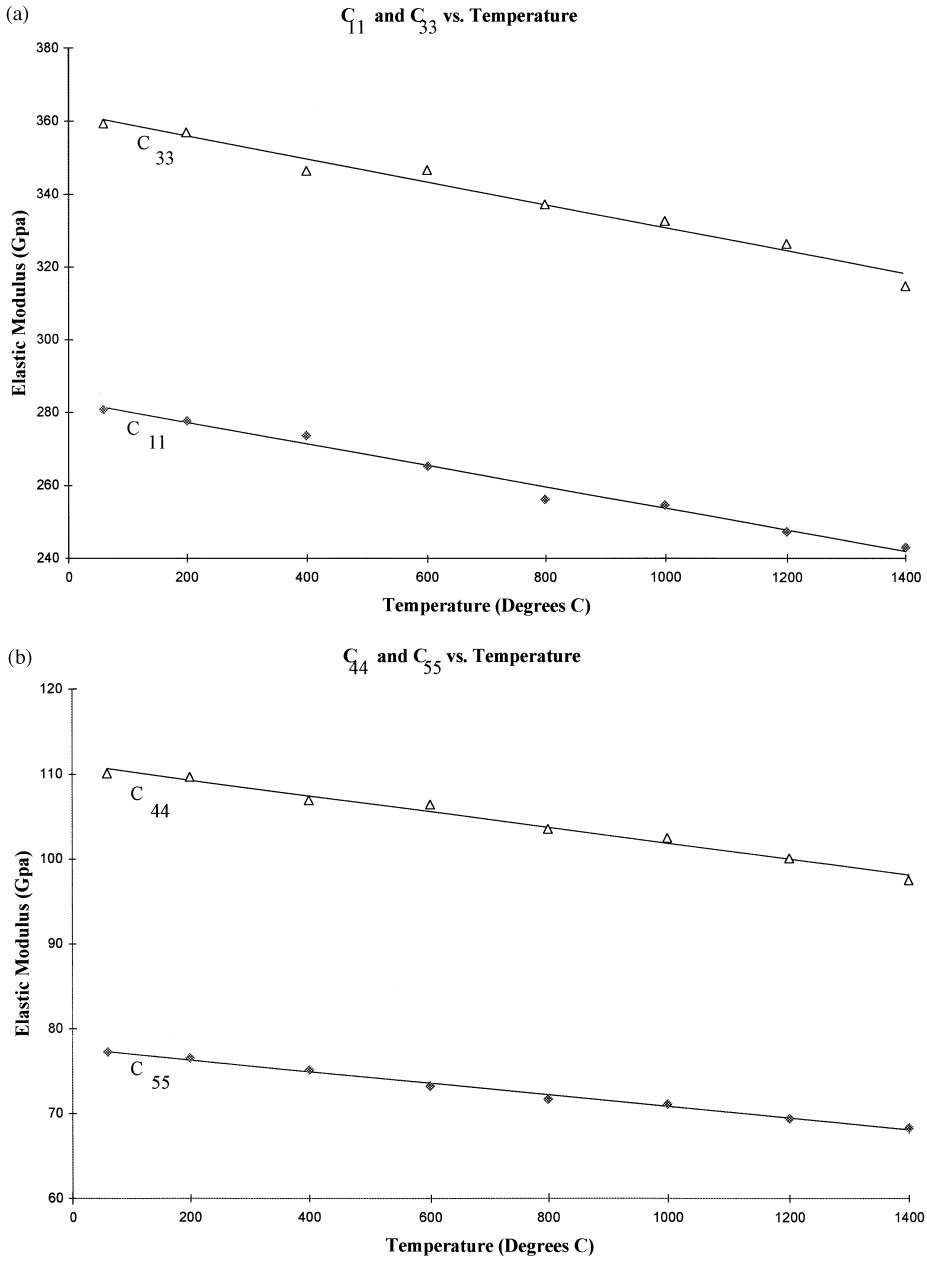

Fig. 6. Variation of selected elastic moduli with temperature.

5 Conclusions

In this work, the lattice parameters and thermal expansion coefficients for stoichiometric mullite ($3Al_2O_3{\cdot}2SiO_2$) powder were measured by X-ray diffractometry up to 900 °C. The data was analyzed by the Rietveld technique, and the strutural discontinuity reported by Schneider *et al.*[12] was confirmed. The temperature range of its occurrence was narrowed to between 425 and 450 °C.

A dense, hot pressed sample of the same mullite made from hydrothermally grown, stoichiometric $3Al_2O_3{\cdot}2SiO_2$ powder was examined by high temperature neutron diffraction and Rietveld analysis. Specimens were cycled from room temperature to 1650 °C, yielding a complete set of axial lattice parameters and thermal expansion coefficients.

In addition, the as-hot pressed, grey mullite (thought to be oxygen deficient due to hot pressing in a graphite die under vacuum) exhibited higher lattice parameters than did those of the (presumably) fully oxidized, white mullite specimen examined in subsequent heating cycles after effectively annealing in air. This observation suggests that the highly incommensurately modulated structure is highly sensitive to oxygen vacancies, and this is the subject of further ongoing work.

Cameron and others[3,33,34] define the position of satellite reflections as being determind by structural vacancies needed to accommodate composition. Thus it follows that additional vacancies will be expected to strongly impact this feature. This observation may have general ramifications in that it suggests that lattice parameters and properties of

oxygen deficient oxide ceramics may differ from those of fully oxygenated, stoichiometric oxides.

The single crystal elastic constants were measured for a melt-grown, orthorhombic, mullite fiber. The complete set of nine elastic moduli were obtained at room temperature, while incomplete measurements up to 1400 °C indicated roughly a 10% drop in stiffness at elevated temperatures.

Acknowledgements

W. M. Kriven gratefully acknowledges the Institut für Kristallographie und Angewandte Mineralogie, in München, Germany, for hosting her sabbatical leave of six months in 1997. The work of J. W. Palko was supported in the United States, by a Fannie and John Hertz Foundation graduate Fellowship. The X-ray work in conjunction with the elastic constant measurements was carried out at the Center for Microanalysis of Materials at UIUC. The WDS electron microprobe analysis was conducted by Dr. I. Steele at the University of Chicago. This work was partially supported by a United States Air Force Office of Scientific Research AASERT Grant, under Contract number F49620-97-1-0427.

References

1. Schneider, H., Okada, K. and Pask, J. A., *Mullite and Mullite Ceramics*. John Wiley, Chichester, UK, 1994.
2. Aksay, I. A. and Pask, J. A., Stable and metastable equilibria in the system SiO_2–Al_2O_3. *J. Am. Ceram. Soc.*, 1975, **58**(11–12), 507–512.
3. Kriven, W. M. and Pask, J. A., Solid solution range and microstructures of melt-grown mullite. *J. Am. Ceram. Soc.*, 1983, **66**(9), 649–654.
4. Sayir, A. and Farmer, S. C. Directionally solidified mullite fibers. In *Ceramic Matrix Composites—Advanced High Temperature Structural Materials. Mat. Res. Soc. Symp. Proc.*, Vol. 365, 1995, pp. 11–20.
5. Wilson, D. M., Lieder, S. L. and Lueneburg, D. C., Microstructure and high temperature properties of NEXTEL 720 fibers. *Cer. Eng. Sci. Proc.*, 1995, **16**, 1005–1012.
6. Göring, J. and Schneider, H., Creep and subcritical crack growth of Nextel 720 alumino silicate fibers as-received and after heat treatment at 1300°C. *Cer. Eng. Sci. Proc.*, 1997, **18**(3), 95–102.
7. Schneider, H., Göring, J., Schmücker, M. and Flucht, F., Thermal stability of Nextel 720 alumino silicate fibers. In *Ceramic Microstructure: Control at the Atomic Level*, ed. A. P. Tomsia and A. Glaeser. Plenum Press, New York, 1998, pp. 721–730.
8. Kriven, W. M., Jilavi, M. H., Zhu, D., Weber, J. K. R., Cho, B., Felten, J. and Nordine, P. C., Synthesis and microstructure of mullite fibers grown from deeply undercooled melts. In *Ceramic Microstructure: Control at the Atomic Level*, ed. A. Glaeser and A. P. Tomsia. Plenum Press, New York, 1998, pp. 169–176.
9. Weber, J. K. R., Cho, B., Hixon, A. D. Abadie, J. G., Nordine, P. C., Kriven, W. M., Johnson, B. R. and Zhu, D., Growth and crystallization of YAG and mullite-composition glass fibers. *J. Euro. Ceram. Soc.*, 1999, **19**(13–14) this issue.
10. Oehlschlegel, G., Kockel, A. and Biedl, A., Anisotrope Mischkristallbildung einiger Verbindungen des ternären Systems BaO–Al_2O_3–SiO_2. Teil II. Messungen an Strukturen mit zweidimensionaler Verknüpfung von $(Si,Al)O_4$-Tetrahederen und Modellvorstellungen von deren Wärmedehnungsanisotropie (Anisotropic mixed crystal formation of a compoundfrom the ternary system BaO–Al_2O_3–SiO_2. Part II. Measurement of structures with two dimensional joining of $(Si,Al)O_4$-tetrahedra and proposed model of their thermal expansion anisotropy). *Glastech. Ber.*, 1974, **47**, 31–41 (in German).
11. Winter, S. and Ghose, S., Thermal expansion and high-temperature crystal chemistry of Al_2SiO_5 polymorphs. *Am. Mineral*, 1979, **64**, 573–586.
12. Schneider, H. and Eberhard, E., Thermal expansion of mullite. *J. Am. Ceram. Soc.*, 1990, **73**, 2073–2076.
13. Margalit, J., Thermal expansion of mullite up to 1500 °C. Ph.D. thesis, Verlag Mainz, Wissenschaftsverlag, Aachen, Germany, 1993 (in German).
14. Schneider, H., Rodewald, K. and Eberhard, E., Thermal expansion discontinuities of mullite. *J. Amer. Ceram. Soc.*, 1993, **76**, 2896–2898.
15. Brunauer, G., Boysen, H., Frey, F., Hansen, T. and Kriven, W. M., High temperature crystal structure of a 3:2 mullite from neutron diffraction data. In preparation.
16. Fenstermacher, J. E. and Hummel, F. A., High temperature mechanical properties of ceramic materials: IV, sintered mullite bodies. *J. Am. Ceram. Soc.*, 1961, **44**(6), 284–289.
17. Davis, R. F. and Pask, J. A., Mullite. In *High Temperature Oxides*, Vol. 4., ed. A. M. Alper. Academic Press, New York, 1971, pp. 37–76.
18. Ledbetter, H., Kim, S., Crudele, S. D. and Kriven, W. M., Elastic properties of mullite. *J. Am. Ceram. Soc.*, 1998, **81**(4), 1025–1028.
19. Sanderock, J. R., Trends in Brillouin scattering: studies of opaque materials, supported films, and central modes. In *Topics in Applied Physics 51, Light Scattering in Solids III: Recent Results*, ed. G. Guntherodt, M. Cardona. Springer-Verlag, New York, 1982, pp. 173–206.
20. Zouboulis, E. S. and Grimsditch, M., Refractive index and elastic properties of MgO up to 1900 K. *J. Geophysical Res.*, 1991, **96**, 4167–4170.
21. Landau, L. D. and Lifshitz, E. M., *Theory of Elasticity. A Course of Theoretical Physics*, Vol. 7. Pergammon Press, London, 1959.
22. Proc. Int'l. Workshop on Oxide/Oxide Composites, Irsee, Bavaria, Germany, 22–24 June 1998. *J. Euro. Ceram. Soc.*, in press.
23. Crudele, S. D., Processing and characterization of alumina platelet-reinforced mullite composites. M.S. thesis, University of Illinois at Urbana-Champaign, 1989.
24. Lorenz, G., Neder, R. B., Marxreiter, J., Frey, F. and Schneider, J., A mirror furnace for neutron diffraction up to 2300 K. *J. Appl. Crystallogr.*, 1993, **26**, 632–635.
25. Sinogeikin, S. V., Bass, J. D. and Katsura, T., Sound velocities and elastic properties of Fe-bearing wadsleyite and ringwoodite. *J. Geophys. Res.*, in press.
26. Weidner, D. J. and Carleton, H. R., Elasticity of coesite. *J. Geophysical Res.*, 1977, **82**(8), 1334–1346.
27. Balzar, D. and Ledbetter, H., Crystal structure and compressibility of 3:2 mullite. *Am. Mineralogist*, 1993, **78**, 1192–1196.
28. Boysen, H., Anharmonic thermal parameters, disorder and phase transition. In *Accuracy in Powder Diffraction II*, ed. E. Prince and J. K. Stalick. NIST, Washington, DC, 1992, pp. 165–174.
29. Thomas, M. W. and Bendall, P. J., A suite of programs for total profile refinement of number of powder diffraction patterns. *Acta Crystallogr.*, 1978, **A34**, 351.

30. Rahman, S. H., Real crystal structure of mullite. In *Mullite and Mullite Ceramics*. John Wiley, Chichester, UK, 1994, pp. 4–31.
31. Palko, J. E., Kriven, W. M., Sinogeikin, S., Bass, J. D. and Sayir, A., Single crystal elastic moduli of mullite. In preparation.
32. Vaughn, M. T. and Weidner, D. J., The relationship of elasticity and crystal structure in andalusite and sillimanite. *J. Phys. Chem. Minerals*, 1978, **3**, 1–12.
33. Cameron, W. E., Composition and cell dimensions of mullite. *Ceram. Bull*, 1977, **56**(11), 1003–1007, 1011.
34. Cameron, W. E., *Amer. Miner.*, 1977, **62**, 747–755.